

Metal Oxyhydroxide Catalysts Promoted CO₂ Absorption and Desorption in Amine-Based Carbon Capture: A Feasibility Study

Long Ji, Jiabi Li, Rongrong Zhai, Jinyi Wang, Xiaolong Wang, Shuiping Yan, and Ming Hua*

Cite This: *ACS Omega* 2022, 7, 44620–44630

Read Online

ACCESS |



Metrics & More

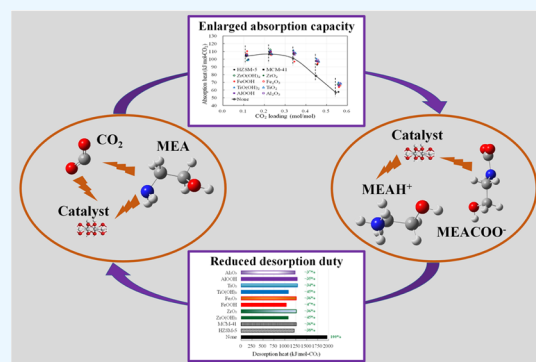


Article Recommendations



Supporting Information

ABSTRACT: The huge energy penalty of CO₂ desorption is the greatest challenge impeding the commercial application of amine-based CO₂ capture. To deal with this problem, a series of metal oxide and oxyhydroxide catalysts were synthesized in this study to kinetically facilitate the CO₂ desorption from 5.0 M monoethanolamine (MEA). The effects of selected catalysts on CO₂ absorption kinetics, CO₂ absorption capacity, CO₂ reaction enthalpy, and desorption duty reduction of 2.0 M MEA were investigated by a true heat flow reaction calorimeter to access the practical feasibility of the catalytic CO₂ desorption. The kinetic study of catalytic CO₂ desorption was also carried out. CO₂ desorption chemistry, catalyst characterization, and structure–function relationships were investigated to reveal the underlying mechanisms. Results show that addition of the catalyst had slight effects on the CO₂ absorption kinetics and CO₂ reaction enthalpy of MEA. In contrast, the CO₂ desorption efficiency greatly increased from 28% in reference MEA to 52% in ZrO(OH)₂-aided MEA. Compared to the benchmark catalyst HZSM-5, ZrO(OH)₂ exhibited a 13% improvement in CO₂ desorption efficiency. More importantly, compared to the reference MEA, the CO₂ desorption duties of ZrO(OH)₂ and FeOOH-aided MEA significantly reduced by 45 and 47% respectively, which are better than those of most other reported catalysts. The large surface area, pore volume, pore diameter, and amount of surface hydroxyl groups of ZrO(OH)₂ and FeOOH afforded the catalytic performance by promoting the adsorption of alkaline speciation (e.g., MEA and HCO₃[−]) onto the particle surface.



1. INTRODUCTION

The continuously generated CO₂ emission by industrial activities is the major contributor to the global temperature increase and climate change.^{1,2} A variety of carbon capture, utilization, and storage technologies, such as chemical absorption,³ membrane separation,^{4,5} solid adsorption,⁶ and CO₂ mineralization,^{7–9} have been developed to mitigate global CO₂ emissions. Amine-based CO₂ capture is the most promising technology due to its technical maturity and features suitable for larger CO₂ emitters. The two commercial applications of this technology in Boundary Dam (Saskatchewan, Canada)¹⁰ and Washington Parish (Texas)¹¹ power plants represent significant progress and potential growth in the future. Also, the application of this technology for natural gas and biogas upgrading not only cuts down CO₂ emissions but also promotes the utilization efficiency of the product and increases the energy profit.¹²

However, amine-based CO₂ capture is still suffering from the intensive energy penalty of CO₂ desorption accounting for >50% of the total energy consumption of CO₂ capture. For instance, coupling the monoethanolamine (MEA)-based capture process to a coal combustion power station would lead to 25–40% efficiency reduction and 70–100% cost elevation in electricity production.¹³ Intensive research has focused on improving the energy efficiency of CO₂ capture and

reducing the energy penalty of CO₂ desorption by novel solvent formula innovation and process intensification. For example, tertiary or sterically hindered amines that have low heat of CO₂ desorption are normally blended with primary or secondary amines that have high CO₂ absorption kinetics to reduce the overall CO₂ desorption heat of the combined solvents.^{14,15} In addition, by reducing the sensible heat and latent heat of CO₂ desorption, the process intensification combined with absorber intercooling, rich splitting, and stripper interheating can achieve an overall energy consumption of 0.3 mW h/t-CO₂ in the MEA-based process, which is 8–20% lower than the conventional configuration.^{16,17} Although these attempts have made great progress in reducing the energy consumption of CO₂ capture, thermodynamic analysis indicates that a further reduction of the energy consumption is theoretically possible (0.2 mW h/t-CO₂).¹⁸

Received: May 8, 2022

Accepted: September 12, 2022

Published: November 29, 2022



Recently, increasing attention has been focused on the development of catalysts/additives to facilitate the desorption kinetics and improve the desorption efficiency, thereby reducing the heat duty of CO₂ desorption. CO₂ desorption involves two key steps: MEAH⁺ deprotonation and MEACOO⁻/HCO₃⁻/CO₃²⁻ breakdown.¹⁹ The difficulty of transferring a proton from MEAH⁺ to other alkaline speciation in a CO₂-loaded MEA solution and the decomposition of MEACOO⁻ contributes to the high energy requirement of CO₂ desorption. There are two promising approaches to facilitate CO₂ desorption apart from temperature elevation: introducing abundant acid or alkaline medium to the solution. Our previous IAM process^{20,21} followed the latter approach and introduced alkaline industrial wastes to the CO₂-lean sorbent to provide hydroxyl, which shifted the chemical equilibrium of the sorbent and converted MEACOO⁻/HCO₃⁻ into free MEA and CO₃²⁻. Li et al.^{22,23} reported catalytic CO₂ desorption by introducing transition metal ions (e.g., Cu²⁺ and Ni²⁺) to MEA–CO₂ solution to form a homogeneous catalysis system, in which metal ions acted as Lewis acids. The results indicated that although the sensible heat and latent heat were not significantly affected by the catalysts, the CO₂ reaction enthalpy reduced from 86.7 kJ/mol-CO₂ in the MEA solution to 71.5 kJ/mol-CO₂ at a Cu²⁺/MEA ratio of 0.1. The metal ions can react with free MEA to form metal–MEA complexes, which act as a chemical heat buffer in CO₂ absorption and desorption. The heat released by CO₂ absorption is stored in the complexes as chemical energy and then liberated in CO₂ desorption, which leads to the decreased CO₂ reaction enthalpy. However, the potentially increased degradation in the presence of metal ions should be further studied before practical application. Alternatively, recent studies^{24–27} reported the utilization of zeolites (e.g., HZSM-5, HY, HX, MCM-41, and SBA-15) and metal oxides (e.g., Al₂O₃, ZrO₂, TiO₂, SiO₂, and ZnO) in a heterogeneous catalysis system to facilitate the kinetics of CO₂ desorption and reduce the heat duty. Bhatti et al.^{28,29} investigated the kinetics of CO₂ desorption from MEA solution catalyzed by several transition metal oxides (V₂O₅, MoO₃, WO₃, TiO₂, and Cr₂O₃). They observed the elevated desorption rate and reduced desorption temperature. Liang and Zhang et al.^{30–33} and Gao et al.²⁴ systematically investigated the catalytic performance of various zeolites, metal oxides, sulfated metal oxides, and metal-modified zeolites. In these previous studies, approximately 10–34% desorption duty reductions and 10–94% CO₂ desorption improvements were achieved for the 5 M MEA solution. Lai et al.³⁵ observed the drastically increased CO₂ desorption rate catalyzed by nanostructured titanium oxyhydroxide (TiO(OH)₂).³⁶

Despite this important progress, there are still knowledge gaps requiring to be filled. Since the concept of catalyst-aided CO₂ desorption is relatively novel and previous studies just focused on limited catalysts, further investigations are required to screen better catalysts and demonstrate the technical and economic feasibility. Iron/zirconium/titanium/aluminum-based oxyhydroxides were widely studied in the wastewater treatment area to catalyze the degradation of organic pollutants due to the high stability of these oxyhydroxides and their abundant active sites to most organic contaminant. Nevertheless, the utilization of metal oxyhydroxides in catalytic CO₂ desorption was not fully investigated. Also, the underlying mechanisms were still not fully understood, especially the correlation of catalyst properties with the CO₂ desorption

performance. The previous studies³⁰ implied that the proton transfer was highly affected by the amount and strength of surface hydroxyls on the surface of catalysts. Particularly, the proton transfer displayed a linear dependence on the Bronsted site-to-Lewis site ratio. However, there are very limited studies on the effects of catalyst properties on catalytic performance by influencing the speciation adsorption onto the particle surface. Considering that both the adsorption of reactants and the proton transfer were supposed to play important roles in CO₂ desorption, it is therefore very important to explore the adsorption of alkaline speciation onto the catalyst surface during CO₂ desorption. In addition, although the desorption duty reduction was measured for various catalysts, the CO₂ reaction enthalpy of the catalyst–amine system was seldom reported in the open literature, and further direct evidence is still demanded to reveal which one in CO₂ reaction enthalpy, sensible heat, or latent heat was actually affected by catalysts.

To fill the abovementioned knowledge gaps, a series of catalysts, iron/zirconium/titanium/aluminum oxyhydroxides (FeOOH, ZrO(OH)₂, TiO(OH)₂, and AlOOH) and iron/zirconium/titanium/aluminum oxides (Fe₂O₃, ZrO₂, TiO₂, and Al₂O₃), were experimentally fabricated in the present study to investigate the improvement for CO₂ absorption and desorption. MEA is the amine that is widely accepted as the benchmark solvent for CO₂ absorption and mineralization due to its simplest chemical structure and typical physicochemical properties. The performance of catalyst-added MEA solution in CO₂ absorption and desorption was first investigated by a true heat flow reaction calorimeter, as well as the measurement of CO₂ reaction enthalpy and desorption duty. The CO₂ desorption of MEA solutions with different catalysts was carried out and compared to highlight the advanced performance. The major speciation of the CO₂-rich and CO₂-lean solutions was identified to verify the reaction pathway. The adsorption experiment of alkaline speciation onto the catalyst surface and catalyst characterization were then conducted to investigate the correlations of catalyst properties with CO₂ desorption performance and to further explore the underlying mechanism of catalytic CO₂ desorption.

2. MATERIALS AND METHODS

2.1. Materials. MEA (≥99%), zirconyl chloride octahydrate (ZrOCl₂·8H₂O, ≥98%), titanium(IV) isopropoxide (TTIP, C₁₂H₂₈O₄Ti, ≥95%), and urea (CH₄N₂O, ≥99%) were purchased from Shanghai Macklin Biochemical Co., Ltd. Iron(III) nitrate nonahydrate (Fe(NO₃)₃·9H₂O, ≥98.5%), aluminum nitrate nonahydrate (Al(NO₃)₃·9H₂O, ≥99%), and sodium hydroxide (NaOH, ≥96%) were purchased from Sinopharm Chemical Reagent Co., Ltd. Zeolite catalysts including HZSM-5 and MCM-41 were purchased from the Catalyst Plant of Nankai University. CO₂ (99.9% purity) and N₂ (99.99% purity) were purchased from Nanjing Tianze Gas Co., Ltd., China.

2.2. Catalyst Fabrication and Characterization. FeOOH and AlOOH catalysts were prepared at 25 °C in polyethylene bottles by dropwise adding 2.0 M NaOH into 0.15 M Fe(NO₃)₃/Al(NO₃)₃ until pH 12 at a stirring rate of 500 rpm.^{36,37} The precipitates were then aged at 90 °C in an oil bath for 48 h. ZrO(OH)₂ was prepared in polyethylene bottles by adding 12 g of urea to 200 mL of 0.15 M ZrOCl₂. The precursor was then stirred at 500 rpm and maintained a temperature at 90 °C in an oil bath for 48 h.^{38–40} After about 4 h, precipitates were gradually formed. TiO(OH)₂ was prepared

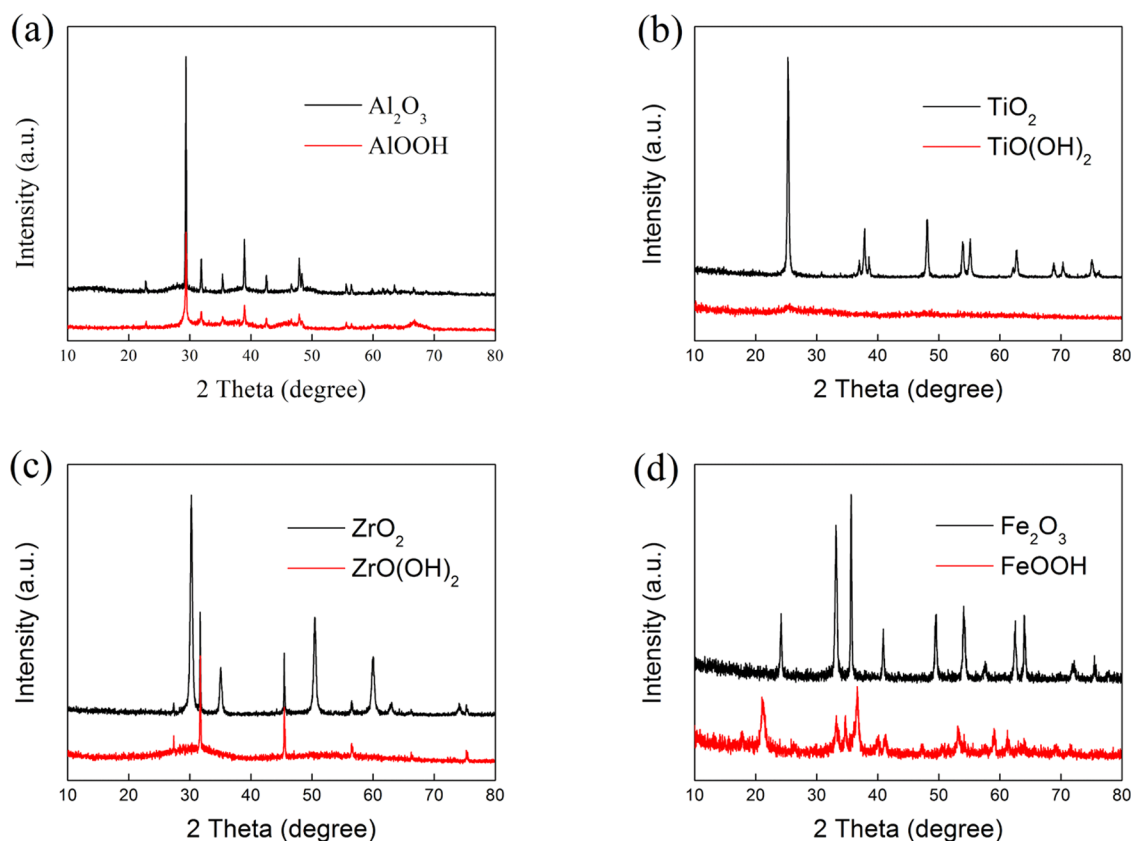


Figure 1. XRD patterns of the catalysts: (a) Al_2O_3 and AlOOH , (b) TiO_2 and $\text{TiO}(\text{OH})_2$, (c) ZrO_2 and $\text{ZrO}(\text{OH})_2$, and (d) Fe_2O_3 and FeOOH .

at 25 °C by dropwise adding TTIP into ultrapure water until the volume ratio of $\text{H}_2\text{O}/\text{TTIP}$ reached 20:1.³⁴ The suspension was then stirred for 4 h. The particles were collected after centrifugation and washed using ultrapure water three times to remove the possible residues attached to the particle surface. The samples were then freeze-dried for 48 h. ZrO_2 , Fe_2O_3 , TiO_2 , and Al_2O_3 were prepared by calcining $\text{ZrO}(\text{OH})_2$, FeOOH , $\text{TiO}(\text{OH})_2$, and AlOOH at 500 °C for 2 h.

The chemical structure of the solid adsorbents was investigated by in situ attenuated total reflection fourier transform infrared (ATR-FTIR) spectroscopy (Nicolet iS5, Thermo Scientific). The particle distributions of the catalysts were measured by a nanoparticle size and ζ -potential analyzer (ZS90, Malvern). The surface areas and pore distributions of the catalysts were characterized by N_2 adsorption–desorption (Nova3000, Quantachrome). All samples were degassed at 77 °C prior to the adsorption–desorption measurements. The specific surface area was calculated by Brunauer–Emmett–Teller theory (BET). The pore size distribution was calculated by applying the density function theory (DFT) method to the absorption branch of the isotherm curve.

2.3. Absorption/Desorption Heat Measurement. The CO_2 absorption and desorption heat of a 2.0 M MEA solution with 0.5 wt % and without catalysts was measured by a CPA201 true heat flow reaction calorimeter (ChemiSens). The photograph of the experimental setup is shown in Figure S1 in the Supporting Information. For each experiment, 100 mL of the 2.0 M MEA solution was filled into a reactor made of glass and stainless steel with an effective volume of 250 mL. The reactor was vacuumed to about -1.0 bars to remove impurities and check for any possible leak. During the CO_2 absorption,

the reactor was submerged in a thermostated liquid bath, and the thermostated liquid was kept at the same temperature (40 °C) as the reactor content. The heat transport from the reactor to the surrounding heat sink was only allowed through the base plate.⁴¹ The reactor temperature sensor controls the Peltier element used as a heat pump to generate the necessary temperature gradients for the heat flow. Five rounds of CO_2 gas were introduced into the reactor via a Bronkhorst mass flow controller with an accuracy of $\pm 0.8\%$ to allow the CO_2 absorption from the gas phase to the MEA solution. The injected CO_2 amount was set as 1.0 g for each injection and 5.0 g in total. For each injection, once the maximum deviation in the pressure and true heat flow was stabilized and the deviations were below ± 0.01 bar and ± 0.02 W, respectively, for 500 s, another round of CO_2 was injected into the reactor. During the CO_2 absorption process, the internal temperature, true heat flow, CO_2 flow rate, and gas pressure (measured using a pressure transducer from Nobel Elektronik Sweden with an accuracy of $\pm 1.0\%$) were recorded every 10 s automatically by a computer. The CO_2 absorption amount, CO_2 loading, and average CO_2 absorption rate were calculated by “CCReport.exe” software based on the CO_2 flow rate and gas pressure signals (with an uncertainty of $\pm 2.0\%$). After five cycles of CO_2 injection, the reactor temperature was accelerated to 99 °C for CO_2 desorption at a rising rate of 1 °C/min. The temperature was maintained at 99 °C for 1800 s. After the desorption experiment, the sorbent was collected and tested by a total organic carbon analyzer (TOC-L, Shimadzu) to determine the CO_2 loading. The true heat flow curve was integrated over the duration to determine the total amount of heat transferred during the CO_2 absorption (with an uncertainty of $\pm 2.3\%$) and CO_2 desorption of CO_2 (with an

Table 1. Physical Properties of the Catalysts

	HZSM-5	MCM-41	Al ₂ O ₃	AlOOH	TiO ₂	TiO(OH) ₂	ZrO ₂	ZrO(OH) ₂	Fe ₂ O ₃	FeOOH
surface area (m ² /g)	319.5	696.4	16.8	5.0	21.0	392.9	29.9	115.2	25.9	87.6
pore volume (cm ³ /g)	0.172	0.661	0.038	0.012	0.091	0.294	0.220	0.230	0.101	0.440
average pore diameter (nm)	2.2	3.8	8.9	9.4	17.4	3.0	29.4	8.0	15.6	20.1
average particle size (nm)	1901	1442	98	424	102	370	160	215	209	260

uncertainty of $\pm 3.9\%$). The detailed description of the calculation method of CO₂ reaction enthalpy and desorption duty refers to Svensson et al.⁴¹ The original data of experiments by CPA201 are given in the Supporting Information.

2.4. Kinetic Experiment of Catalytic CO₂ Desorption.

Considering that the CPA201 reactor did not support sampling during the desorption experiment and the reactor was open during the desorption experiment, which hindered the calculation of desorption performance based on the pressure, individual desorption experiments were conducted in this section. The schematic diagram of the experimental setup is given in Figure S2 in the Supporting Information. For each experiment, the CO₂-rich solution was prepared in a bubble column with an internal volume of 250 mL. The mixed gas with a CO₂ concentration of 15% and a gas flow rate of 1.7 L/min was prepared using CO₂/N₂ mass flow controllers (D07-7B, Sevenstar) and humidified in a column filled with water before contacting with 150 mL of the 5.0 M MEA solution. The solution was maintained at 40 °C by a circulating water bath. The CO₂-rich solution was then transferred into a three-necked flask for the CO₂ desorption test. For each experiment, the rich solution was introduced with a 1 wt % catalyst, stirred at 500 rpm, heated up from 30 to 99 °C, and maintained at 99 °C by an oil bath with atmospheric pressure. Since previous studies indicated that the CO₂ loading of the MEA solution became stable within 180 min at similar operating conditions,^{28–33} the experimental duration was set as 180 min in this study; 2 mL of slurry samples were extracted at different reaction times and were immediately filtered through a 0.2 μm nylon syringe filter. The filtrate was treated by a total organic carbon analyzer (TOC-L, Shimadzu) to determine the CO₂ loading. The pH value of the filtrate was measured by a pH meter (FE28, Mettler Toledo, Switzerland). An ATR-FTIR (Tensor 27, Bruker) was used to determine the major speciation in the filtrate. Prior to the analysis of the speciation of the filtrate, the baseline was adjusted to zero. Two independent experiments were performed for each catalyst. The original data of experiments by a three-necked flask are given in the Supporting Information.

2.5. Adsorption Experiment of Alkaline Speciation.

The adsorption of MEA-bearing species and HCO₃⁻ onto catalyst particles was carried out at 298 K in a 250 mL conical flask with a 0.5 g/L catalyst dosage. For each measurement, the reaction solution was prepared by adding CO₂-rich MEA (the solution was prepared following the same procedure mentioned in Section 2.4) or NaHCO₃ into ultrapure water until a carbon concentration of 100 mg/L. The suspension was then shaken for 24 h in an incubator shaker to achieve adsorption equilibrium. The suspension sample was then extracted and immediately filtered through a 0.2 μm nylon syringe filter. The filtrate was treated by a total organic carbon analyzer (TOC-L, Shimadzu) to determine the residual amount of alkaline species in the solution. The adsorption

amount of alkaline species was therefore the amount change before and after catalyst dosing.

3. RESULTS AND DISCUSSION

3.1. Catalyst Characterization. Figure 1a–d shows the X-ray diffraction (XRD) results of eight catalysts used in the present study. The absence of typical crystalline peaks and broad background signals in XRD patterns of four metal oxyhydroxide catalysts indicated their poorly crystallized nature.⁴² In contrast, the four metal oxide catalysts (ZrO₂, Fe₂O₃, TiO₂, and Al₂O₃) after the calcination treatment of their corresponding oxyhydroxides at 500 °C displayed typical crystallization phases indicated by their several diffraction peaks in XRD patterns. Previous studies^{42–44} indicated that the metal oxyhydroxide with a noncrystallized structure likely represented high surface area, large pore volume, and even rich surface functional groups. The cluster particle size distributions (Figure S3) show that the catalysts produced were nearly monodisperse in size. The average diameter results (Table 1) indicate that the metal oxides (50–200 nm) were smaller than the metal oxyhydroxides (200–450 nm). The cluster decreased particle size of the metal oxides is due to further condensation reactions of the surface hydroxyl groups occurring during 500 °C calcination, which is consistent with the previous study.⁴³ This phenomenon is also in agreement with the FTIR results shown in Figure 2, where metal oxyhydroxides exhibited obviously higher peak intensity of surface groups than metal oxides. Particularly, the peak at 1380 cm⁻¹ corresponds to hydroxyl groups on the particle surface.⁴⁴

N₂ sorption analysis was used to investigate the porosity properties of the catalysts. Representative sorption isotherms obtained for the catalysts are shown in Figure S4. All sorption

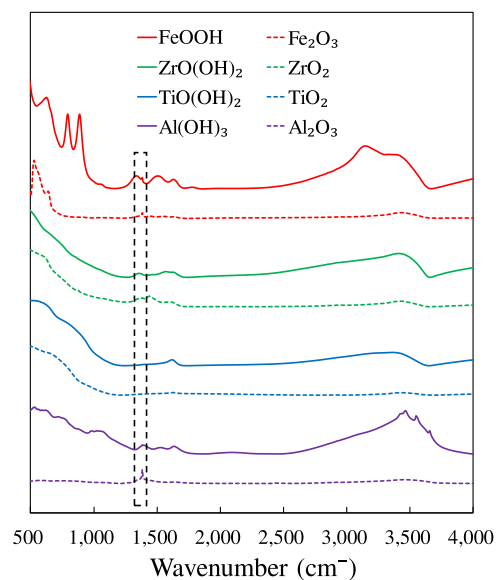


Figure 2. FTIR spectra of the catalysts.

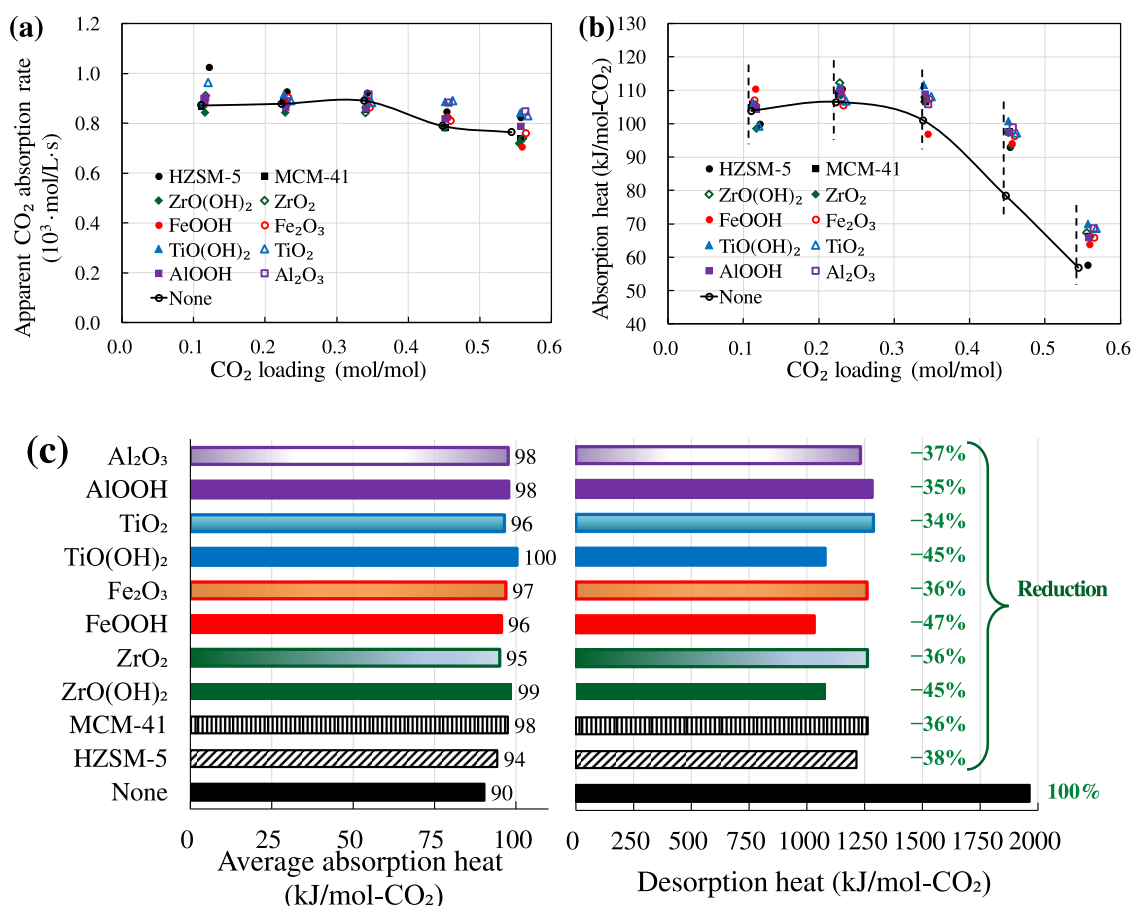


Figure 3. Effects of selected catalysts on CO₂ absorption and desorption in 5 M MEA: (a) apparent CO₂ absorption rate as a function of CO₂ loading, (b) absorption heat as a function of CO₂ loading, and (c) the average absorption and desorption heat. Detailed data for Figure 3a–c can be seen in Tables S1 and S2.

isotherms were typical Type IV with hysteresis loops, indicating the presence of mesopores (2–50 nm) on the particle surface. All catalysts used in this study presented <30 nm average pore sizes (Table 1), which were supposed to be favored for adsorption and catalysis reactions.⁴³ Also, the onset of high N₂ uptake at low relative pressure indicated the presence of micropores (<2 nm), which was more pronounced in HZSM-5, MCM-41, TiO(OH)₂, ZrO(OH)₂, and FeOOH. In addition, TiO(OH)₂, ZrO(OH)₂, and FeOOH displayed larger pore volumes than their corresponding oxides (Table 1). More specifically pore size distributions were calculated by applying the density function theory (DFT) method on the adsorption branch of the isotherm curve, as shown in Figure S5. The smaller pore volumes of ZrO₂ and TiO₂ than those of ZrO(OH)₂ and TiO(OH)₂ are probably due to the collapse of micropores after the 500 °C calcination treatment. The smaller pore volume of Fe₂O₃ than that of FeOOH likely resulted from the collapse of 15–30 nm mesopores. Differently, the pore volume increased from 0.012 cm³/g of AlOOH to 0.038 cm³/g of Al₂O₃ after calcination (Table 1). Moreover, the specific surface area of the catalyst can be calculated based on N₂ sorption results by Brunauer–Emmett–Teller (BET) theory, which was significantly influenced by the difference in crystallinity and the pore size and pore structure.⁴² TiO(OH)₂ exhibited the highest surface area among all catalysts because of its abundant micropores, as shown in Figure S5c. As expected, metal oxides displayed smaller surface areas than

their corresponding oxyhydroxides except for Al₂O₃ (Table 1), attributed to the collapse of micropores and crystallization in the calcination treatment.

3.2. Effects of Selected Catalysts on CO₂ Absorption and Desorption in 2.0 M MEA. To confirm the feasibility of catalytic CO₂ desorption, the effects of selected catalysts on CO₂ absorption kinetics, absorption capacity, reaction enthalpy, and desorption duty reduction in 5 M MEA were investigated by a true heat flow reaction calorimeter. Figure 3a shows apparent CO₂ absorption rates of 5 M MEA with and without catalysts as a function of CO₂ loading. For each experiment, 5 g of CO₂ was injected into the reactor in five cycles with 1 g of CO₂ injected for each cycle. CO₂ loading of MEA increased from about 0.11 mol-CO₂/mol-MEA in the first cycle to about 0.55 mol-CO₂/mol-MEA in the fifth cycle. The apparent CO₂ absorption rates decreased in the five cycles because the amount of free MEA for CO₂ absorption decreased as CO₂ loading increased. Notably, the addition of catalysts led to a slight increase in the apparent CO₂ absorption rate compared to the reference MEA, except for ZrO(OH)₂ in the first cycle, ZrO(OH)₂ and AlOOH in the second cycle, Fe₂O₃, ZrO₂, and AlOOH in the third cycle, and Fe₂O₃, FeOOH, ZrO₂, ZrO(OH)₂, and MCM-41 in the fifth cycle. A similar phenomenon was observed in previous studies. For example, Lee et al.^{45,46} reported that the CO₂ absorption rate of the methanol absorbent decreased by 9% in the presence of Al₂O₃ nanoparticles and increased by 8% in the

presence of SiO₂ nanoparticles. It is proven that the gas–liquid mass transfer can be enhanced by suitable nanoparticles. Krishnamurthy et al.⁴⁷ observed a faster dye diffusion in nanoparticle suspensions compared to that in the base fluid. Wang et al.⁴⁸ investigated the overall mass transfer coefficient of MEA with SiO₂ or Al₂O₃ nanoparticles in a wetted-wall column and found that the micro convective motion contributed to about 80% of the increased CO₂ diffusivity in the liquid phase, which supports the reliability of the shuttle effect and the boundary mixing effect. However, the underlying mechanism of the enhancement of nanoparticles for CO₂ absorption was not fully understood and required further investigation.

Apart from the apparent CO₂ absorption rate, the addition of different catalysts also affected the CO₂ absorption capacity. As shown in Figure 3a, MEA with catalysts exhibited higher CO₂ loading compared to the reference MEA system without catalysts after five cycles of CO₂ injection. For example, MEA with ZrO₂, ZrO(OH)₂, and HZSM-5 achieved CO₂ loadings of 0.560, 0.555, and 0.557 mol/mol respectively, which was slightly higher than the reference MEA (0.544 mol/mol). The possible reason might be the adsorption of CO₂ onto the particle surface of the catalyst by the surface pores via van der Waals force and the hydroxyl group via internal coordination.⁴⁹ Similarly, Galhotra⁴⁹ reported the adsorption of CO₂ by Al₂O₃ and the formation of carbonate on the surface particle, contributing to the enlarged CO₂ loading. It is well known that the adsorption capacity depended on the number of active sites or active surfaces. Although most of the selected catalysts possessed high surface areas, the low catalyst dosage (0.5 wt %) led to a slight increase in CO₂ loading.

Figure 3b shows the CO₂ reaction enthalpy of 5 M MEA with and without catalysts as a function of CO₂ loading, while Figure 3c shows the corresponding averaged CO₂ reaction enthalpy after five cycles of CO₂ absorption. The reference MEA exhibited a CO₂ reaction enthalpy of 90 kJ/mol-CO₂, which is very close to the value simulated by the validated Aspen Plus modeling (90.3 kJ/mol-CO₂)²³ and the value reported by Li et al. (86.7 kJ/mol-CO₂).²² The dosing of catalysts afforded a larger CO₂ reaction enthalpy compared to the reference MEA without catalysts. The slightly increased CO₂ reaction enthalpy likely resulted from the larger CO₂ loading in catalyst–MEA solutions. In addition, the CO₂ reaction enthalpy of catalyst–MEA solutions increased slightly as the CO₂ loading increased from about 0.1 to about 0.35 mol/mol, while it always decreased for the reference MEA without catalysts during the same CO₂ loading range. The reason for this observation might be the adsorption of MEA species on the catalyst, which was an endothermic reaction.¹⁸

Figure S6 shows the very similar energy inputs for CO₂ desorption of MEA with and without catalysts. Compared to the MEA without catalysts, adding catalysts can reduce the overall CO₂ desorption duty (Figure 3c) by releasing more CO₂ (Table S2) without additional energy input. Specifically, compared to the reference MEA system in the absence of a catalyst, CO₂ desorption duty was reduced by 45% with 0.5 wt % ZrO(OH)₂ as a catalyst and reduced by 47% in the presence of 0.5 wt % FeOOH. In contrast, the zeolites have milder effects, with CO₂ desorption duty reduction of 33 and 36% for HZSM-5 and MCM-41, respectively.

3.3. CO₂ Desorption Performance of Catalysts. The effects of selected catalysts on CO₂ desorption performance were assessed with two important process indicators: CO₂

loading and pH value. The other two indicators, cyclic CO₂ loading and CO₂ desorption efficiency, can be calculated based on CO₂ loading.¹⁹ In Figure 4a, for 5 M MEA solutions with or without catalysts, the CO₂ loading decreased as a function of reaction time during CO₂ desorption. The CO₂ loading decreased rapidly in the first 30 min, attributed to the fast decomposition of bicarbonate (HCO₃⁻). This result can be confirmed by the rapidly decreased intensity of the FTIR peak of HCO₃⁻ in Figure 5. After 30 min, the solution temperature

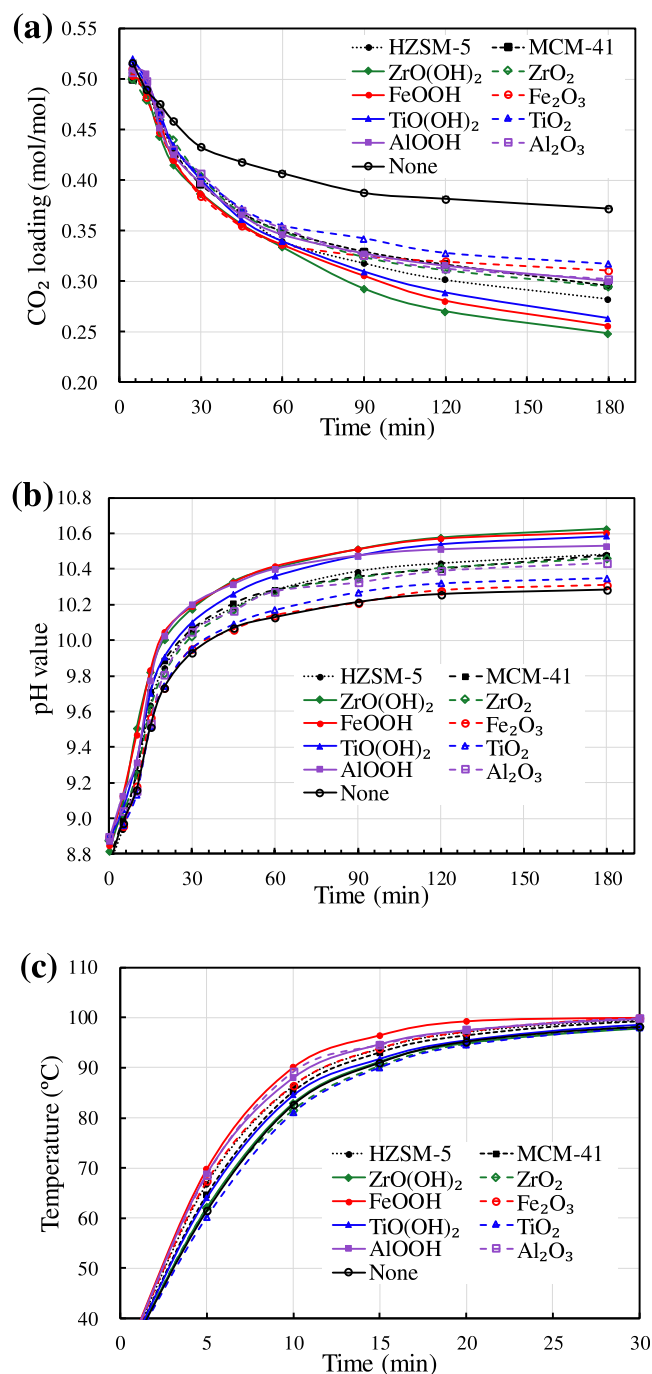


Figure 4. Catalytic CO₂ desorption performance in the 5 M MEA solution with and without different catalysts at 99 °C. The weight ratio of the catalyst to MEA solution is 1 wt %: (a) CO₂ loading curves along with time, (b) pH value curves along with time, and (c) temperature curves along with time.

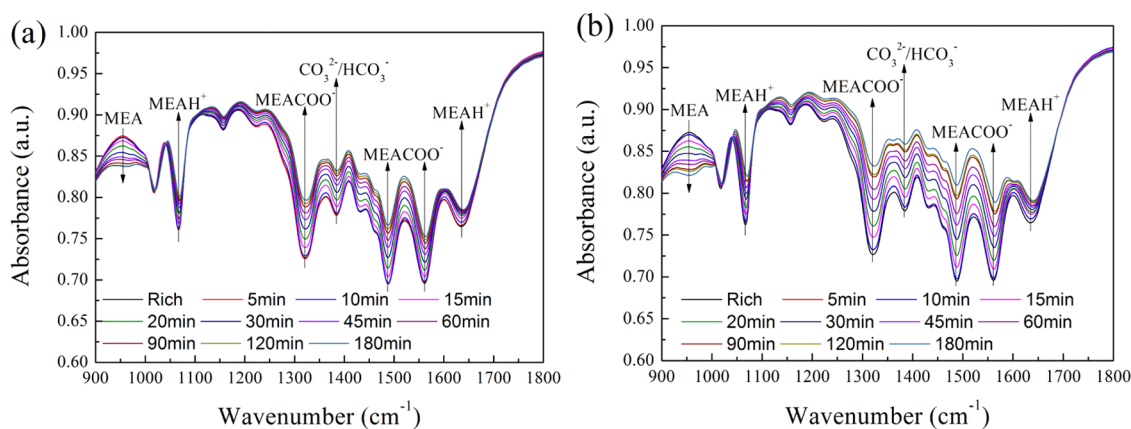


Figure 5. In situ FTIR spectra of the 5 M MEA solution during CO₂ desorption at 99 °C: (a) without catalysts and (b) with 1 wt % HZSM-5 as a catalyst.

Table 2. Summary of the Cyclic Loading (the CO₂ Loading Change before and after CO₂ Desorption) and Desorption Efficiency of the 5.0 M MEA Solution with and without Different Catalysts at 99 °C^a

parameters	none	TiO ₂	Fe ₂ O ₃	Al ₂ O ₃	AlOOH	MCM-41	ZrO ₂	HZSM-5	TiO(OH) ₂	FeOOH	ZrO(OH) ₂
cyclic loading (mol/mol)	0.148	0.203	0.209	0.218	0.220	0.224	0.225	0.238	0.257	0.265	0.272
desorption efficiency (%)	28	39	40	42	42	43	43	46	49	51	52

^aThe weight ratio of the catalyst to MEA solution is 1 wt %.

reached 99 °C and the CO₂ loading decreasing rate slowed slightly. At this stage, the composition of the carbamate (MEACOO⁻) became the dominating reaction of CO₂ desorption. Compared to the reference MEA solution without catalysts, catalyst-aided MEA displayed faster kinetics of CO₂ desorption, resulting in larger cyclic CO₂ loading and CO₂ desorption efficiency (Table 2) after 3 h of the desorption reaction. For example, CO₂ desorption efficiency and cyclic loading increased from 28% and 0.148 mol/mol in the catalyst-free MEA solution to 46% and 0.238 mol/mol, respectively, in the HZSM-5 aided MEA solution, which is close to the data reported in previous studies.³¹ The enhancement of catalysts for CO₂ desorption was in the following order: ZrO(OH)₂ > FeOOH > TiO(OH)₂ > HZSM-5 > ZrO₂ > MCM-41 > AlOOH > Al₂O₃ > TiO₂ > none. Also, HZSM-5 displayed faster kinetics of CO₂ desorption than MCM-41, ZrO₂, Fe₂O₃, TiO₂, and Al₂O₃, which is consistent with the results reported by previous studies.^{24,31} In those studies, HZSM-5 exhibited better improvement of CO₂ desorption than many other commercial zeolites (e.g., HY, HX, MCM-41, and SBA-15) and metal oxides (e.g., Al₂O₃, ZrO₂, TiO₂, SiO₂, and ZnO) due to its high surface area and a large amount of acid hydroxyls.³¹ HZSM-5 was therefore accepted as a benchmark catalyst for CO₂ desorption. In addition, three metal oxyhydroxides, ZrO(OH)₂, FeOOH, and TiO(OH)₂, exhibited much faster kinetics than their corresponding metal oxides and even HZSM-5. Faster CO₂ desorption kinetics then resulted in larger cyclic CO₂ loading and CO₂ desorption efficiency. Among the selected catalysts, ZrO(OH)₂ achieved the best enhancement for CO₂ desorption: 52% CO₂ desorption efficiency and 0.272 mol/mol cyclic loading (Table 2).

The corresponding pH value curves of MEA solutions with HZSM-5 and without catalysts in Figure 4b confirmed the above observation. The pH values of the reference MEA solution increased from 8.7 to 10.3 in CO₂ desorption as a function of time, while the increasing trend of MEA solutions with catalysts is noticeably more significant. For example, the

pH values of the HZSM-5-aided MEA solution increased from 8.7 to 10.5 after CO₂ desorption reactions, indicating a higher CO₂ desorption efficiency compared to the reference MEA. Moreover, the phenomenon can also be confirmed by the FTIR results shown in Figure 5a,b. The peaks of COO⁻ asymmetric stretching at 1568 cm⁻¹, symmetric stretching at 1486 cm⁻¹, and N-COO⁻ stretching vibration at 1322 cm⁻¹ were assigned to MEA carbamate (MEACOO⁻).⁵⁰⁻⁵² A typical absorption peak at 1388 cm⁻¹ corresponding to doubly degenerate stretching was assigned to carbonate (CO₃²⁻).⁵⁰ The -COO⁻ symmetric stretching at 1360 cm⁻¹ was assigned to bicarbonate (HCO₃⁻).⁵² The C-N-H out-of-plane wagging and C-NH₂ twisting at 955 cm⁻¹ corresponded to free MEA, while the N-H rocking at 1634 cm⁻¹ and C-N stretching at 1069 cm⁻¹ were identified as the protonated MEA (MEAH⁺).⁵¹ As CO₂ desorption goes on, the peak intensities of MEACOO⁻, HCO₃⁻, and CO₃²⁻ of the reference MEA decreased rapidly, reflecting the decomposition of this speciation and the release of CO₂. The free MEA peak at 955 cm⁻¹ was enlarged after CO₂ desorption reactions, while the MEAH⁺ peak at 1069 cm⁻¹ decreased and the other MEAH⁺ peak at 1634 cm⁻¹ shifted to 1645 cm⁻¹. This result confirmed the deprotonation of MEAH⁺ and the regeneration of free MEA and CO₂. As expected, the intensity change of speciation peaks is noticeably more significant in the MEA-catalyst system than that in the catalyst-free MEA, confirming the higher CO₂ desorption efficiency afforded by catalysts.

Figure 4c shows the increased temperature as a function of time in the kinetic experiments of catalytic CO₂ desorption of 5 M MEA solutions with or without catalysts. Compared to the reference MEA without catalysts, catalyst-aided MEA displayed a faster rate of temperature increase in CO₂ desorption, except for ZrO₂ and TiO₂. It is clear that the thermal conductivity of the MEA solution was changed by dosing nanoparticles. The enhancement of catalysts for temperature increase displayed the following order: FeOOH > Al₂O₃ > AlOOH > Fe₂O₃ > HZSM-5 > MCM-41 > TiO(OH)₂ > ZrO(OH)₂ > none. The

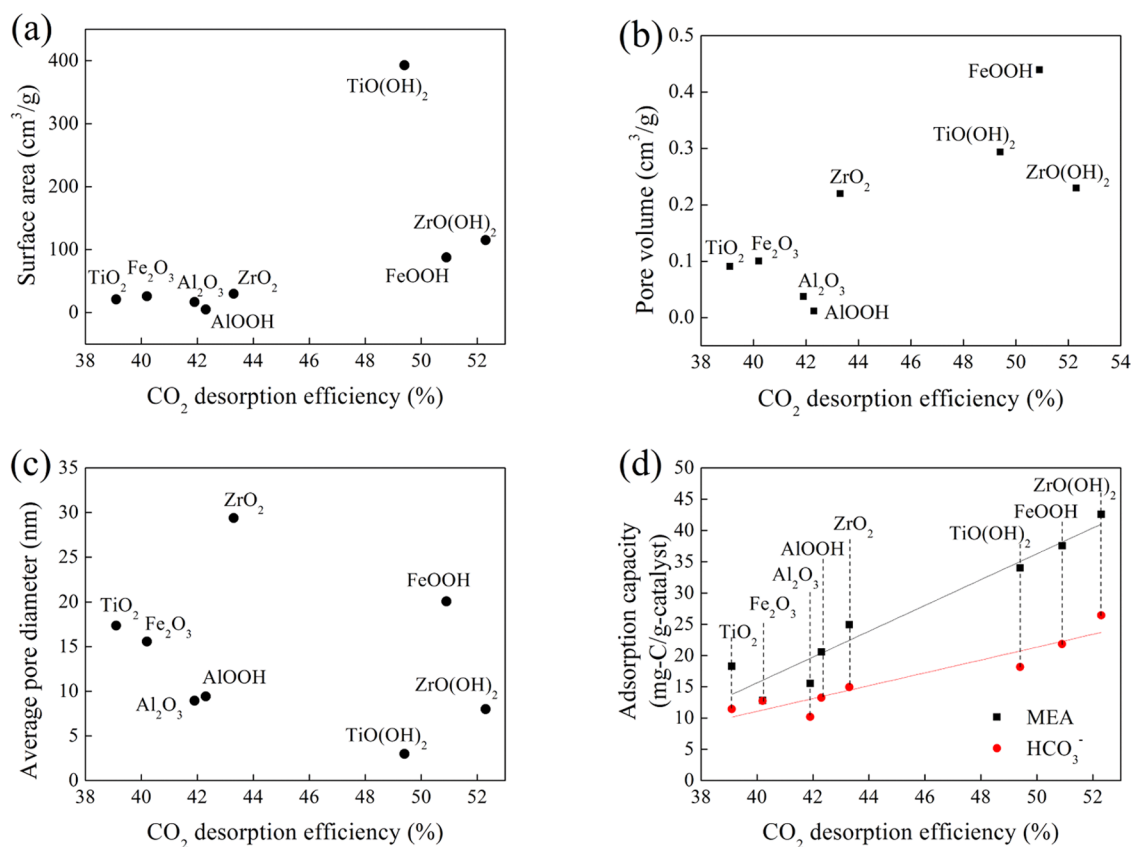


Figure 6. Relationships between CO₂ desorption efficiency and catalyst properties: (a) surface area, (b) pore volume, (c) average pore diameter, and (d) adsorption capacity.

large thermal conductivity of the catalyst facilitated the heat transfer from the heat source to the MEA solution. A similar phenomenon was also reported in the previous study by Lee et al.,^{45,46} in which Al₂O₃ and SiO₂ displayed obvious enhancement for heat transfer in methanol.

3.4. Mechanisms behind the Catalytic CO₂ Desorption. As mentioned above, different catalysts displayed various CO₂ desorption performances. The mechanisms of catalytic CO₂ desorption can be explained from chemical and physical aspects. The catalytic CO₂ desorption includes several key steps: adsorption of alkaline speciation (such as MEACOO⁻/HCO₃⁻/CO₃²⁻) onto the active sites of the catalyst particles, the proton transfer occurring on the particle surface, and the generation and detachment of the CO₂ bubbles. The CO₂ desorption performance could be affected by several catalyst properties such as surface acid hydroxyls, surface area, pore volume, and pore diameter. Correlations between the CO₂ desorption efficiency with catalyst properties were conducted in this study to explore the underlying mechanism. As illustrated in Figure 6a,b, the three oxyhydroxides TiO(OH)₂, ZrO(OH)₂, and FeOOH with larger surface areas and pore volumes exhibited much higher CO₂ desorption efficiency compared to their corresponding metal oxides. Large surface area and pore volume not only contributed to the adsorption of alkaline speciation onto the catalyst but also provided more space available for the following proton transfer and thus promoted the CO₂ desorption efficiency.^{30,43} Besides the physical adsorption, the more abundant acid hydroxyls of TiO(OH)₂, ZrO(OH)₂, and FeOOH than their corresponding metal oxides also contributed to the better catalytic performance through chemisorption. In particular, the acid hydroxyl

not only benefited alkaline speciation adsorption as an active site but also provided a proton to the adsorbed speciation.²⁴ The effect of acid hydroxyls has been reported by Zhang et al.,³⁰ in which a nearly linear dependency was observed between catalytic performance with surface area and the Bronsted site-to-Lewis site ratio. Notably, AlOOH displayed a higher CO₂ desorption efficiency than Al₂O₃, although Al₂O₃ has a larger surface area and pore volume. The noncorrelated trend might be more significantly affected by the larger amount of acid hydroxyl of AlOOH than that of Al₂O₃. In Figure 6c, although the CO₂ desorption efficiency displayed independence to catalyst pore diameters, a more correlated relationship can be found between CO₂ desorption efficiency with catalyst pore distributions. Compared to other catalysts, TiO(OH)₂ and ZrO(OH)₂ displayed smaller pore diameters, which contributed to their high CO₂ desorption efficiency by enhancing the physisorption to alkaline speciation. Although FeOOH owned a large pore diameter, the presence of micropores contributed to its high CO₂ desorption efficiency through physisorption to alkaline speciation.

Adsorption experiments of alkaline speciation (MEA and HCO₃⁻) onto catalysts were then conducted to confirm the combination effect of surface area, pore volume, and pore diameter on CO₂ desorption efficiency. Although MEACOO⁻ is also alkaline speciation, it cannot individually exist in the solution. Therefore, just the adsorption of MEA and HCO₃⁻ onto the catalysts was investigated in this study. Adsorption capacities, $q_{\max\text{-MEA}}$ and $q_{\max\text{-HCO}_3^-}$, were used to access the adsorption performance of catalysts toward MEA and HCO₃⁻, respectively. In Figure 6d, CO₂ desorption efficiency displayed

an obvious linear correlation with the adsorption capacities of catalysts to alkaline speciation of MEA and HCO_3^- . This result clearly confirmed the combined effect of surface area, pore volume, and pore diameter on CO_2 desorption efficiency via adsorption. Besides the adsorption provided by particle surface, micro/mesopores, and acid hydroxyls, the coordination of unsaturated metal sites of catalyst particles could also be the active sites. Once adsorbed, the alkaline speciation then accepted protons from acid hydroxyls. For example, a zwitterion (MEACOOH) is formed when MEACOO^- accepts a proton from the acid hydroxyl. The actual reaction pathway may be much more complex. The N atom is sp^3 hybridized in MEA and MEACOOH , but it is sp^2 hybridized in MEACOO^- .⁵³ Besides proton transfer, the molecular structure change should also occur in CO_2 desorption reactions. Unfortunately, it is very difficult to experimentally monitor the in situ reactions of the alkaline speciation occurring on the surface of catalyst particles. The DFT computational simulation reported by Idem et al.²⁴ indicated that a coordination unsaturated metal atom of catalyst particles, which is likely a Lewis acid site, could attract the O atom of the N– CO_2 plane of MEACOO^- via the chemisorption process. A neighboring acid hydroxyl attaches to the other O atom of the N– CO_2 plane and donates a proton to the O atom, and the proton then shifts to the N atom of the N– CO_2 plane to construct MEACOOH .^{30–32} Another neighboring metal site could attach to the N atom of the N– CO_2 plane by attracting the lone pair of electrons of the N.²⁴ Attributing to the stretching of the metal sites, the configuration of the N atom would be transferred from sp^2 to sp^3 and the strength of the C–N bond would also be weakened to facilitate CO_2 desorption. After giving protons, the acid hydroxyl became an alkaline site and could then adsorb acid speciation from the solution such as MEA^+ . The acid hydroxyl can be recovered by grabbing a proton from MEA^+ . Meanwhile, free MEA was regenerated through this process. Without an acid catalyst, the proton transfer and the N–C bond stretching/breakdown rely only on external heat supplies.

Besides the effect on alkaline speciation decomposition, catalyst particles would also influence heat transfer and CO_2 bubble generation and detachment. Catalyst particles were dispersed in MEA solution by mechanical stirring, and some particles would contact the heat transfer surface between the heating source and MEA solution. The large surface area of catalyst particles increased the heat transfer surface area. Also, the nanoparticles contacting the heated surface would become bubble generation points and promote bubble generation by providing microsites and an irregular surface.⁴⁵ The generated CO_2 bubbles then aggregated and became larger. As the buoyancy of the large bubble increased more than the adhesive force between the particle and the bubble, bubble detachment would happen. Lee et al.⁴⁶ reported that the CO_2 bubbles were more easily generated and desorbed from the boiling surface in the presence of Al_2O_3 particles than that in the reference water. In addition, most metal oxides or oxyhydroxides possessed larger thermal conductivities than MEA solution, which could also enhance the heat transfer from the heating source to the MEA solution.

4 CONCLUSIONS

In this study, a series of metal oxide and oxyhydroxide catalysts were synthesized to kinetically facilitate CO_2 desorption from 5 M MEA. The effects of selected catalysts on CO_2 absorption

and desorption performance, as well as the underlying mechanisms, were investigated. Results show that adding catalysts had slight effects on the CO_2 absorption kinetics and CO_2 reaction enthalpy of MEA. In contrast, the CO_2 desorption efficiency greatly increased from 28% in reference MEA to 52% in $\text{ZrO}(\text{OH})_2$ -aided MEA. Compared to the benchmark catalyst HZSM-5, $\text{ZrO}(\text{OH})_2$ exhibited a 13% improvement in CO_2 desorption efficiency. More importantly, compared to the reference MEA, the CO_2 desorption duties of $\text{ZrO}(\text{OH})_2$ and FeOOH -aided MEA significantly reduced by 45 and 47%, respectively, which are better than those of most other reported catalysts. The large surface area, pore volume, pore diameter, and amount of surface hydroxyl groups of $\text{ZrO}(\text{OH})_2$ and FeOOH afforded the catalytic performance by promoting the adsorption of alkaline speciation (e.g., MEA and HCO_3^-) onto the particle surface.

While catalyst-aided CO_2 desorption is a promising alternative technology for the energy penalty reduction of amine-based CO_2 capture, more detailed studies should be conducted to investigate any potential problems. The effects of impurities in flue gases, such as O_2 and H_2O , and even heavy metals on the performance stability of catalyst-aided CO_2 desorption should be explored in future works. The recycling possibility, cyclic performance stability, and unavoidable loss of the catalyst should also be further investigated in the long-term and multicycle experiments.

ASSOCIATED CONTENT

Supporting Information

The Supporting Information is available free of charge at <https://pubs.acs.org/doi/10.1021/acsomega.2c02851>.

Photograph of the experimental setup of the CPA201 true heat flow reaction calorimeter (Figure S1); schematic diagram of the experiment setup (Figure S2); cluster particle size of the selected catalyst in 5 M MEA (Figure S3); N_2 physisorption isotherms of selected catalysts (Figure S4); pore size distribution calculated from their desorption branch of N_2 physisorption isotherms (Figure S5); temperature and true heat flow curves of 5 M MEA with and without the catalyst during CO_2 desorption (Figure S6); detailed data for Figure 3a,b (Table S1); and detailed data for Figure 3c (Table S2) (PDF)

Original data of experiments by CPA201 (XLSX)

AUTHOR INFORMATION

Corresponding Author

Ming Hua – State Key Laboratory of Pollution Control and Resource Reuse, School of the Environment, Nanjing University, Nanjing 210023, China; orcid.org/0000-0001-6871-7196; Phone: +86-13913871197; Email: huaming@nju.edu.cn

Authors

Long Ji – State Key Laboratory of Pollution Control and Resource Reuse, School of the Environment, Nanjing University, Nanjing 210023, China; College of Engineering, Huazhong Agricultural University, Wuhan 430070, China; orcid.org/0000-0003-0816-298X

Jiabi Li – State Key Laboratory of Pollution Control and Resource Reuse, School of the Environment, Nanjing University, Nanjing 210023, China

Rongrong Zhai – School of Energy Power and Mechanical Engineering, North China Electric Power University, Beijing 102206, China; orcid.org/0000-0001-5020-6187

Jinyi Wang – Huaneng Clean Energy Research Institute, Beijing 102209, China

Xiaolong Wang – Huaneng Clean Energy Research Institute, Beijing 102209, China

Shuiping Yan – College of Engineering, Huazhong Agricultural University, Wuhan 430070, China

Complete contact information is available at:

<https://pubs.acs.org/10.1021/acsomega.2c02851>

Notes

The authors declare no competing financial interest.

ACKNOWLEDGMENTS

L.J. greatly appreciates the financial support from the Major Science and Technology Program for Water Pollution Control and Treatment (Grant No. 2017ZX07204001).

REFERENCES

- (1) Boot-Handford, M. E.; Liu, Q.; Xu, Z.; Zeng, H.; et al. Carbon capture, and storage update. *Energy Environ. Sci.* **2014**, *7*, 130–189.
- (2) Yu, B.; Li, L.; Yu, H.; Maeder, M.; Puxty, G.; Yang, Q.; Feron, P.; Conway, W.; Chen, Z. Insights into the chemical mechanism for CO₂(aq) and H⁺ in aqueous diamine solutions – An experimental stopped-flow kinetic and ¹H/¹³C NMR study of aqueous solutions of N,N-Dimethylethylenediamine for postcombustion CO₂ capture. *Environ. Sci. Technol.* **2018**, *52*, 916–926.
- (3) Rochelle, G. T. Amine scrubbing for CO₂ capture. *Science* **2009**, *325*, 1652–1654.
- (4) Yan, S.; He, Q.; Zhao, S.; Wang, Y.; Ai, P. Biogas upgrading by CO₂ removal with a highly selective natural amino acid salt in gas–liquid membrane contactor. *Chem. Eng. Process.* **2014**, *85*, 125–135.
- (5) Yan, S.; Zhao, S.; Wardhaugh, L.; Feron, P. H. M. Innovative Use of Membrane Contactor as Condenser for Heat Recovery in Carbon Capture. *Environ. Sci. Technol.* **2015**, *49*, 2532–2540.
- (6) Creamer, A. E.; Gao, B. Carbon-based adsorbents for postcombustion CO₂ capture: A critical review. *Environ. Sci. Technol.* **2016**, *50*, 7276–7289.
- (7) Bobicki, E. R.; Liu, Q.; Xu, Z.; Zeng, H. Carbon capture and storage using alkaline industrial wastes. *Prog. Energy Combust. Sci.* **2012**, *38*, 302–320.
- (8) Wang, T.; Huang, H.; Hu, X.; Fang, M.; Luo, Z.; Guo, R. Accelerated mineral carbonation curing of cement paste for CO₂ sequestration and enhanced properties of blended calcium silicate. *Chem. Eng. J.* **2017**, *323*, 320–329.
- (9) Wang, X.; Maroto-Valer, M. M. Integration of CO₂ capture and mineral carbonation by using recyclable ammonium salts. *ChemSusChem* **2011**, *4*, 1291–1300.
- (10) SaskPower, Boundary Dam Carbon Capture Project. <http://www.saskpower.com/our-power-future/carbon-capture-and-storage/boundary-dam-carbon-capture-project/>, 2014.
- (11) Global CCS Institute Projects Database, Petra Nova Carbon Capture. <https://www.globalccsinstitute.com/projects/petra-nova-carbon-capture-project>, 2017.
- (12) Monlau, F.; Sambusiti, C.; Ficara, E.; Aboulkas, A.; Barakat, A.; Carrère, H. New opportunities for agricultural digestate valorization: current situation and perspectives. *Energy Environ. Sci.* **2015**, *8*, 2600–2621.
- (13) Li, K.; Leigh, W.; Feron, P.; Yu, H.; Tade, M. Systematic study of aqueous monoethanolamine (MEA)-based CO₂ capture process: Techno-economic assessment of the MEA process and its improvements. *Appl. Energy* **2016**, *165*, 648–659.
- (14) Muchan, P.; Saiwan, C.; Narku-Tetteh, J.; Idem, R.; Supap, T.; Tontiwachwuthikul, P. Screening tests of aqueous alkanolamine solutions based on primary, secondary, and tertiary structure for blended aqueous amine solution selection in post combustion CO₂ capture. *Chem. Eng. Sci.* **2017**, *170*, 574–582.
- (15) Narku-Tetteh, J.; Muchan, P.; Saiwan, C.; Supap, T.; Idem, R. Selection of components for formulation of amine blends for post combustion CO₂ capture based on the side chain structure of primary, secondary and tertiary amines. *Chem. Eng. Sci.* **2017**, *170*, 542–560.
- (16) Jiang, K.; Li, K.; Yu, H.; Chen, Z.; Wardhaugh, L.; Feron, P. Advancement of ammonia based post-combustion CO₂ capture using the advanced flash stripper process. *Appl. Energy* **2017**, *202*, 496–506.
- (17) Li, K.; Cousins, A.; Yu, H.; Feron, P.; Tade, M.; Luo, W.; Chen, J. Systematic study of aqueous monoethanolamine-based CO₂ capture process: model development and process improvement. *Energy Sci. Eng.* **2016**, *4*, 23–39.
- (18) Li, K.; Jiang, K.; Jones, T. W.; Feron, P. H. M.; Bennett, R. D.; Hollenkamp, A. F. CO₂ regenerative battery for energy harvesting from ammonia-based post-combustion CO₂ capture. *Appl. Energy* **2019**, *247*, 417–425.
- (19) Ji, L.; Yu, H.; Yu, B.; Jiang, K.; Grigore, M.; Wang, X.; Zhao, S.; Li, K. Integrated absorption–mineralisation for energy-efficient CO₂ sequestration: Reaction mechanism and feasibility of using fly ash as a feedstock. *Chem. Eng. J.* **2018**, *352*, 151–162.
- (20) Yu, B.; Yu, H.; Li, K.; Ji, L.; Yang, Q.; Wang, X.; Chen, Z.; Megharaj, M. A Diamine-Based Integrated Absorption–Mineralization Process for Carbon Capture and Sequestration: Energy Savings, Fast Kinetics, and High Stability. *Environ. Sci. Technol.* **2018**, *52*, 13629–13637.
- (21) Ji, L.; Yu, H.; Li, K.; Yu, B.; Grigore, M.; Yang, Q.; Wang, X.; Chen, Z.; Zeng, M.; Zhao, S. Integrated absorption-mineralisation for low-energy CO₂ capture and sequestration. *Appl. Energy* **2018**, *225*, 356–366.
- (22) Li, K.; van der Poel, P.; Conway, W. O.; Jiang, K.; Puxty, G.; Yu, H.; Feron, P. H. M. Mechanism investigation of advanced metal–ion-mediated amine regeneration: a novel pathway to reducing CO₂ reaction enthalpy in amine-based CO₂ capture. *Environ. Sci. Technol.* **2018**, *52*, 14538–14546.
- (23) Cheng, C.-H.; Li, K.; Yu, H.; Jiang, K.; Chen, J.; Feron, P. Amine-based post-combustion CO₂ capture mediated by metal ions: Advancement of CO₂ desorption using copper ions. *Appl. Energy* **2018**, *211*, 1030–1038.
- (24) Idem, R.; Shi, H.; Gelowitz, D.; Tontiwachwuthikul, P. Catalytic Method and Apparatus for Separating a Gaseous Component from an Incoming Gas Stream. US Patent, US9,586,1752017.
- (25) Shi, H.; Naami, A.; Idem, R.; Tontiwachwuthikul, P. Catalytic and non catalytic solvent regeneration during absorption-based CO₂ capture with single and blended reactive amine solvents. *Int. J. Greenhouse Gas Control* **2014**, *26*, 39–50.
- (26) Srisang, W.; Pouryousefi, F.; Osei, P. A.; Decardi-Nelson, B.; Akachuku, A.; Tontiwachwuthikul, P.; Idem, R. Evaluation of the heat duty of catalyst-aided amine-based post combustion CO₂ capture. *Chem. Eng. Sci.* **2017**, *170*, 48–57.
- (27) Wang, T.; Yu, W.; Liu, F.; Fang, M.; Farooq, M.; Luo, Z. Enhanced CO₂ absorption and desorption by monoethanolamine (MEA)-based nanoparticle suspensions. *Ind. Eng. Chem. Res.* **2016**, *55*, 7830–7838.
- (28) Bhatti, U. H.; Shah, A. K.; Kim, J. N.; You, J. K.; Choi, S. H.; Lim, D. H.; Nam, S.; Park, Y. H.; Baek, I. H. Effects of Transition Metal Oxide Catalysts on MEA Solvent Regeneration for the Post-Combustion Carbon Capture Process. *ACS Sustainable Chem. Eng.* **2017**, *5*, 5862–5868.
- (29) Bhatti, U. H.; Nam, S.; Park, S.; Baek, I. H. Performance and Mechanism of Metal Oxide Catalyst-Aided Amine Solvent Regeneration. *ACS Sustainable Chem. Eng.* **2018**, *6*, 12079–12087.
- (30) Zhang, X.; Zhu, Z.; Sun, X.; Yang, J.; Gao, H.; Huang, Y.; Luo, X.; Liang, Z.; Tontiwachwuthikul, P. Reducing Energy Penalty of CO₂ Capture Using Fe Promoted SO₄²⁻/ZrO₂/MCM-41 Catalyst. *Environ. Sci. Technol.* **2019**, *53*, 6094–6102.

- (31) Zhang, X.; Huang, Y.; Gao, H.; Luo, X.; Liang, Z.; Tontiwachwuthikul, P. Zeolite catalyst-aided tri-solvent blend amine regeneration: An alternative pathway to reduce the energy consumption in amine-based CO₂ capture process. *Appl. Energy* **2019**, *240*, 827–841.
- (32) Zhang, X.; Liu, H.; Liang, Z.; Idem, R.; Tontiwachwuthikul, P.; Al-Marri, M. J.; Benamor, A. Reducing energy consumption of CO₂ desorption in CO₂-loaded aqueous amine solution using Al₂O₃/HZSM-5 bifunctional catalysts. *Appl. Energy* **2018**, *229*, 562–576.
- (33) Liang, Z.; Idem, R.; Tontiwachwuthikul, P.; Yu, F.; Liu, H.; Rongwong, W. Experimental study on the solvent regeneration of a CO₂-loaded MEA solution using single and hybrid solid acid catalysts. *AIChE J.* **2016**, *62*, 753–765.
- (34) Gao, H.; Huang, Y.; Zhang, X.; Bairq, Z. A. S.; Huang, Y.; Tontiwachwuthikul, P.; Liang, Z. Catalytic performance and mechanism of SO₄²⁻/ZrO₂/SBA-15 catalyst for CO₂ desorption in CO₂-loaded monoethanolamine solution. *Appl. Energy* **2020**, *259*, No. 114179.
- (35) Lai, Q.; Toan, S.; Assiri, M. A.; Cheng, H.; Russell, A. G.; Adidharma, H.; Radosz, M.; Fan, M. Catalyst-TiO(OH)₂ could drastically reduce the energy consumption of CO₂ capture. *Nat. Commun.* **2018**, *9*, No. 2672.
- (36) Ding, X.; Song, X.; Boily, J.-F. Identification of Fluoride and Phosphate Binding Sites at FeOOH Surfaces. *J. Phys. Chem. C* **2012**, *116*, 21939–21947.
- (37) Bloch, B.; Ravi, B. G.; Chaim, R. Stabilization of transition alumina and grain growth inhibition in ultrafine Al₂O₃–5 wt % SrO alloy. *Mater. Lett.* **2000**, *42*, 61–65.
- (38) Shan, C.; Xu, Y.; Hua, M.; Gu, M.; Yang, Z.; Wang, P.; Lu, Z.; Zhang, W.; Pan, B. Mesoporous Ce-Ti-Zr ternary oxide millispheres for efficient catalytic ozonation in bubble column. *Chem. Eng. J.* **2018**, *338*, 261–270.
- (39) Fang, X.-L.; Li, Y.; Chen, C.; Kuang, Q.; Gao, X.-Z.; Xie, Z.-X.; Xie, S.-Y.; Huang, R.-B.; Zheng, L.-S. pH-Induced Simultaneous Synthesis and Self-Assembly of 3D Layered β-FeOOH Nanorods. *Langmuir* **2010**, *26*, 2745–2750.
- (40) Watanabe, S.; Ma, X.; Song, C. Characterization of Structural and Surface Properties of Nanocrystalline TiO₂-CeO₂ Mixed Oxides by XRD, XPS, TPR, and TPD. *J. Phys. Chem. C* **2009**, *113*, 14249–14257.
- (41) Svensson, H.; Zejnullahu Velasco, V.; Hultberg, C.; Karlsson, H. T. Heat of absorption of carbon dioxide in mixtures of 2-amino-2-methyl-1-propanol and organic solvents. *Int. J. Greenhouse Gas Control* **2014**, *30*, 1–8.
- (42) Machala, L.; Zboril, R.; Gedanken, A. Amorphous Iron(III) Oxide. *J. Phys. Chem. B* **2007**, *111*, 4003–4018.
- (43) Chee Kimling, M.; Scales, N.; Hanley, T. L.; Caruso, R. A. Uranyl-sorption properties of amorphous and crystalline TiO₂/ZrO₂ millimeter-sized hierarchically porous beads. *Environ. Sci. Technol.* **2012**, *46*, 7913–7920.
- (44) Yang, L.; Hu, C.; Nie, Y.; Qu, J. Surface acidity and reactivity of β-FeOOH/Al₂O₃ for pharmaceuticals degradation with ozone: In situ ATR-FTIR studies. *Appl. Catal., B* **2010**, *97*, 340–346.
- (45) Lee, J. S.; Lee, J. W.; Kang, Y. T. CO₂ absorption/regeneration enhancement in DI water with suspended nanoparticles for energy conversion application. *Appl. Energy* **2015**, *143*, 119–129.
- (46) Lee, J. W.; Torres Pineda, I.; Lee, J. H.; Kang, Y. T. Combined CO₂ absorption/regeneration performance enhancement by using nanoabsorbents. *Appl. Energy* **2016**, *178*, 164–176.
- (47) Krishnamurthy, S.; Bhattacharya, P.; Phelan, P. E.; Prasher, R. S. Enhanced Mass Transport in Nanofluids. *Nano Lett.* **2006**, *6*, 419–423.
- (48) Wang, T.; Yu, W.; Fang, M.; He, H.; Xiang, Q.; Ma, Q.; Xia, M.; Luo, Z.; Cen, K. Wetted-wall column study on CO₂ absorption kinetics enhancement by additive of nanoparticles. *Greenhouse Gases: Sci. Technol.* **2015**, *5*, 682–694.
- (49) Galhotra, P. Carbon Dioxide Adsorption on Nanomaterials. PhD (Doctor of Philosophy) Thesis; University of Iowa, 2010.
- (50) Richner, G.; Puxty, G. Assessing the chemical speciation during CO₂ absorption by aqueous amines using in situ FTIR. *Ind. Eng. Chem. Res.* **2012**, *51*, 14317–14324.
- (51) Robinson, K.; McCluskey, A.; Attalla, M. I. An FTIR spectroscopic study on the effect of molecular structural variations on the CO₂ absorption characteristics of heterocyclic amines. *ChemPhysChem* **2011**, *12*, 1088–1099.
- (52) Robinson, K.; McCluskey, A.; Attalla, M. I. An ATR-FTIR study on the effect of molecular structural variations on the CO₂ absorption characteristics of heterocyclic amines, part II. *ChemPhysChem* **2012**, *13*, 2331–2341.
- (53) Ma, C.; Pietrucci, F.; Andreoni, W. Capture, and Release of CO₂ in Monoethanolamine Aqueous Solutions: New Insights from First-Principles Reaction Dynamics. *J. Chem. Theory Comput.* **2015**, *11*, 3189–3198.